FLUID MECHANICS

Complete measurement of helicity and its dynamics in vortex tubes

Martin W. Scheeler,[1] Wim M. van Rees,[2] Hridesh Kedia,[1] Dustin Kleckner,[1]* William T. M. Irvine[1,3]†

Helicity, a topological measure of the intertwining of vortices in a fluid flow, is a conserved quantity in inviscid fluids but can be dissipated by viscosity in real flows. Despite its relevance across a range of flows, helicity in real fluids remains poorly understood because the entire quantity is challenging to measure. We measured the total helicity of thin-core vortex tubes in water. For helical vortices that are stretched or compressed by a second vortex, we found conservation of total helicity. For an isolated helical vortex, we observed evolution toward and maintenance of a constant helicity state after the dissipation of twist helicity by viscosity. Our results show that helicity can remain constant even in a viscous fluid and provide an improved basis for understanding and manipulating helicity in real flows.

Conserved quantities, such as energy, momentum, and angular momentum, are the foundation of our understanding of the physical world. Tracking their conversion between different forms—for example, potential to kinetic energy—provides deep insight into phenomena from the motion of planets to the production of energy in the Sun. Idealized fluids, which lack viscosity, possess an additional conserved quantity: helicity. Helicity measures the degree to which vortex field lines embedded in a fluid system wind around each other, distinguishing it from its counterparts as a topological feature of the flow (*1*). This topological origin makes helicity a powerful geometric lens for understanding otherwise complex dynamics. For example, in plasmas, magnetic helicity is conjectured to be better conserved than energy in the presence of small dissipation (*2*). This insight has been important not only in understanding natural magnetic field structures, including Earth's magnetosphere (*3*) and the solar corona (*4*), but also in enabling advances in tokamak reactors and similar clean-energy technologies (*5*, *6*).

For classical fluids, however, similar progress is hampered by the influence of viscosity, which can have a dramatic impact on fluid flow, even if present in infinitesimal amounts. In particular, viscosity can destroy the preservation of field-line topology, removing the very mechanism that ensures helicity conservation in ideal, inviscid fluids. As a result, there has been extensive theoretical debate regarding helicity in real fluids, including the extent of its conservation, potential mechanisms for its transfer, and the constraints that these dynamics may impose (*1*, *7*–*15*). In addition to representing an advance in our fundamental understanding of fluids, an understanding of helicity stands to have a tangible impact on a number of difficult problems. In the case of atmospheric flows—for which helicity has already been identified as a good predictor of "supercell" formation (*16*) and aided in explaining the longer lifetimes of these violent storms (*17*)—a better understanding of its dynamics can help connect disparate yet interacting scales that are important in the modeling of tornadogenesis and other natural phenomena (*18*). Furthermore, the topological perspective provided by helicity may help in elucidating the structures and mechanisms present in the formation of turbulence (*19*), where the means by which nonzero helicity reduces the nonlinear energy transfer between scales is still unknown (*20*, *21*).

Gaining experimental insights into helicity dynamics in viscous fluids is challenging, owing to the difficulties in resolving the vorticity field structure across multiple scales. Here we present a technique for sampling vortex core velocities that enables the complete measurement of helicity dynamics in a real fluid. Using this technique, we measured the helicity evolution for two vortex configurations: (i) a helical vortex loop leapfrogging a planar ring and (ii) an isolated helical vortex loop. In each case, the geometry of the vorticity field lines governs the evolution of the helicity in a fundamental way.

We based our investigation on small collections of thin-core vortices (Fig. 1A). Examples of

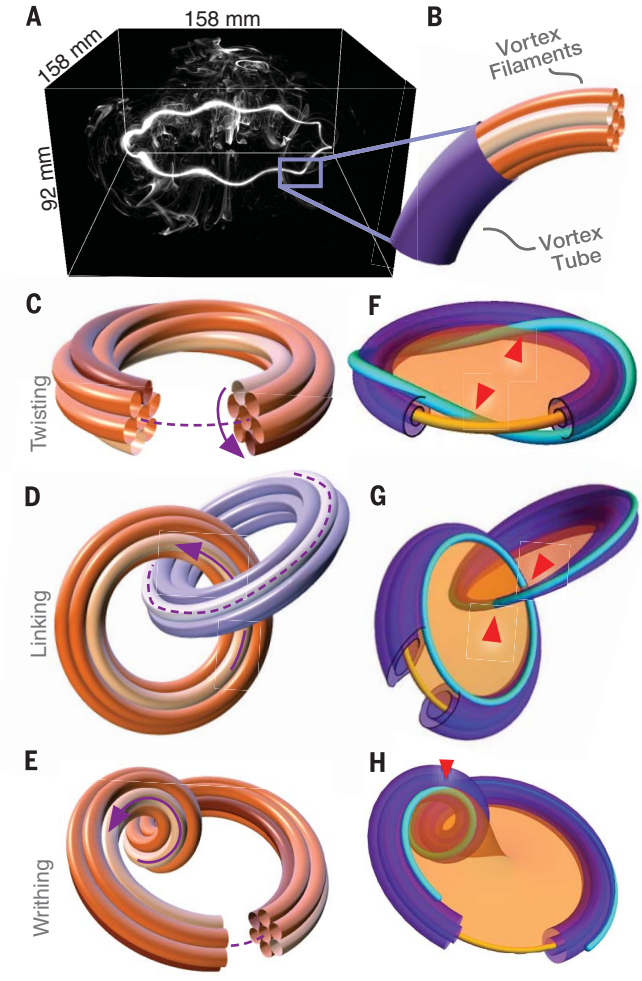

Fig. 1. Modes of helicity storage and their relationship to field-line winding. (**A**) A volumetric image of a helically wound vortex tube generated in water, imaged using high-speed laser-scanning tomography and fluorescent dye. (**B**) A schematic of vortex tube structure, illustrating the presence of many vortex filaments (orange and white tubes) inside a single vortex tube (purple shell). (**C** to **E**) Twisting, linking, and writhing bundles of field lines, respectively, demonstrating the resulting winding of the individual field lines around each other. (**F** to **H**) Twisting, linking, and writhing configurations, respectively, are shown with a single field line highlighted (cyan) in each bundle. Two of the many vortex surfaces nested around the centerline on which the vortex field lines lie are shown (purple), along with a surface spanning the loop (orange). Red arrowheads indicate the locations where the field line pierces the spanning surface.

[1]Department of Physics, The University of Chicago, Chicago, IL 60637, USA. [2]The John A. Paulson School of Engineering and Applied Sciences, Harvard University, Cambridge, MA 02138, USA. [3]James Franck Institute and Enrico Fermi Institute, The University of Chicago, 929 East 57th Street, Chicago, IL 60637, USA.
*Present address: University of California, Merced, 5200 Lake Road, Merced, CA 95343, USA. †**Corresponding author. Email: wtmirvine@uchicago.edu**

commonly encountered thin-core vortices are found in aircraft wakes (*22*, *23*), in insect flight (*24*–*26*), and as the "sinews" of complex flows (*27*–*29*). Such thin-core vortex structures are an ideal model system for studying helicity dynamics, because they allow helicity to be broken into distinct geometric forms. This can be visualized by considering each vortex "tube" as a bundle of individual filaments, analogous to the construction of a twisted rope (Fig. 1B). The ways in which the filaments—and the field lines that they contain—can wind around each other is then limited to a set of three topologically related forms of helicity: twisting, linking, and writhing (movie S1).

Twisting is the local winding of the filaments around the vortex tube centerline (Fig. 1C). Integrating the local twisting along the length of the vortex tube gives the first component of the helicity, known as twist, *Tw*. A second, twist-free mode of storage can be achieved by linking two thin-cored rings (Fig. 1D), providing a contribution to the total helicity that is equal to the sum of the linking numbers, *Lk*.

Even when the vortex field lines are untwisted everywhere and the tubes are unlinked, winding inside a single tube can still be achieved by coiling or writhing the centerline of the tube (Fig. 1E). This final component of the helicity is given by the writhe, *Wr*, which measures the overall rotation accumulated by a locally parallel bundle as it is followed once around the tube. For small coilings, the writhe takes on the value $\phi_{BPC}/2\pi$, where ϕ_{BPC} is the Berry-Pancharatnam-Chiao phase, corresponding to the rotation angle of the linear polarization of light propagating down a coiled optical fiber (*30*–*33*).

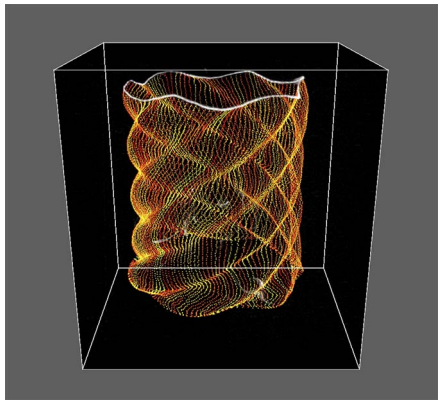

Movie 1. A volumetric movie of an isolated helical vortex evolving in water, whose core has been seeded with dye blobs. The trajectory of each blob is tracked as the vortex evolves and is progressively overlaid on the volume in warm colors.

Geometrically distinct, but topologically equivalent (movie S1), these three forms of winding completely capture the total helicity

$$\mathcal{H} = \int \vec{u} \cdot \vec{\omega} \mathrm{d}V = \sum_{i \neq j} \Gamma_i \Gamma_j Lk_{ij} + \sum_i \Gamma_i^2 (Tw_i + Wr_i) \quad (1)$$

where the integral is performed over all space, and each index labels a vortex tube with vorticity flux (circulation), Γ_i (u, velocity of the fluid; ω, vorticity; dV, a volume element) (*19*, *34*). The equivalence between the volumetric form and the discrete sum of geometric terms depends on the vorticity being organized into vortex tubes. Although the linking and writhe can be deduced from a measurement of the vortex tube centerlines alone (*15*), measuring the twist, and thus the total helicity, requires additionally measuring the flow inside each of the vortex tubes.

For tubes that are sufficiently thin, and whose winding varies minimally across a cross section, the total helicity is encoded completely in the flow along the centerline of the vortex tube. This simplification arises from the fact that each of the vortex field lines that wind around the centerline will necessarily pierce a surface spanning the closed vortex loop (Fig. 1, F to H), generating a vorticity flux through that surface, and thus, by Stoke's law, a flow around its boundary. In this case, we write the helicity in the experimentally accessible form

$$\mathcal{H} = \sum_i \Gamma_i \oint_{\mathcal{C}_i} \vec{u} \cdot d\vec{\ell} \quad (2)$$

where the sum is performed over each tube, $\mathcal{C}_i$ is the centerline of a given tube, and $d\ell$ is a line element (*35*). This form reduces the problem of sampling the vorticity and flow throughout the entire core to tracking the flow along the centerline of each vortex (*36*).

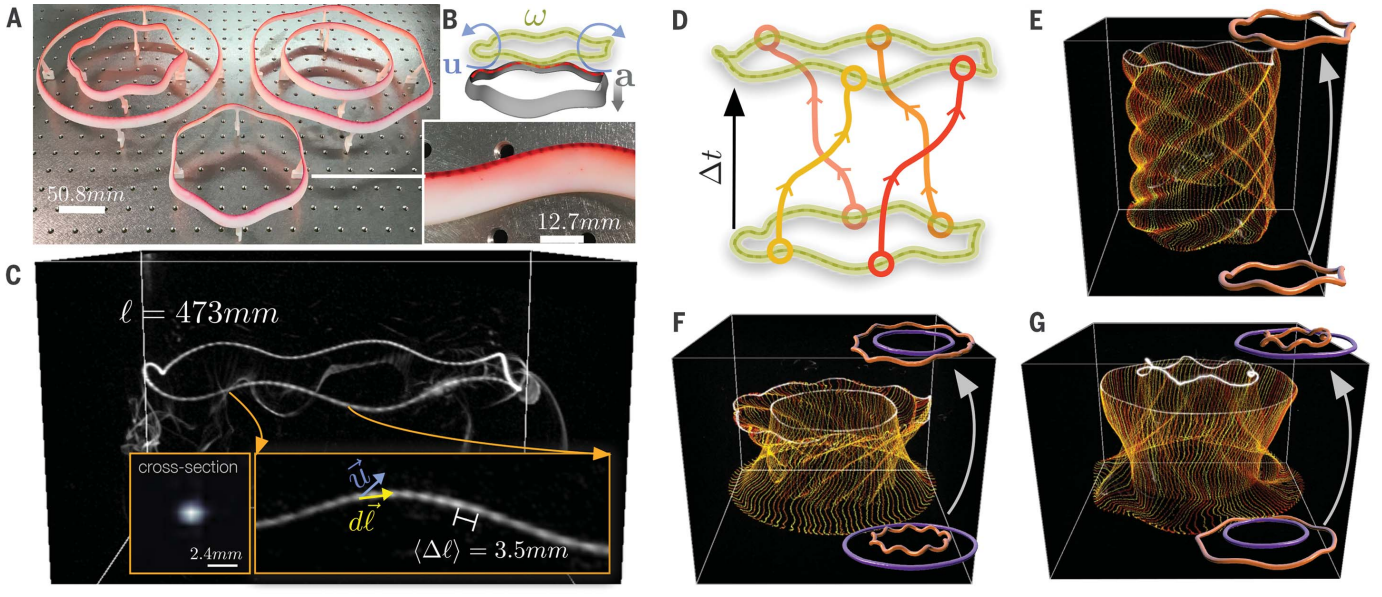

Fig. 2. Technique for experimentally measuring the total helicity of a configuration of thin-core vortices. (**A**) Hydrofoils used to produce vortex configurations. Red coloration results from application of rhodamine dye solution to hydrofoil trailing edges. The inset shows details of dye patterning. (**B**) Schematic of the vortex generation process. The vortex tube (ω), the flow field (u), and the direction of hydrofoil acceleration (**a**, where the red dashed line indicates the side on which dye was applied) are shown. (**C**) Volumetric image of a dyed and patterned helical vortex in water. The inset resolves individual dye blobs inside the core. (**D**) Schematic representation of the dye-blob tracking procedure (t, time). (**E**) Volumetric image of an isolated helical vortex evolving in water (Movie 1), with dye-blob tracks overlaid in warm colors. Cartoons are renderings of traced initial (lower) and final (upper) vortex paths extracted from the volume. (**F** and **G**) Volumetric images of leapfrogging vortices (helix stretching and helix compression, respectively). Cartoons are renderings of traced initial (lower) and final (upper) vortex paths extracted from each experiment.

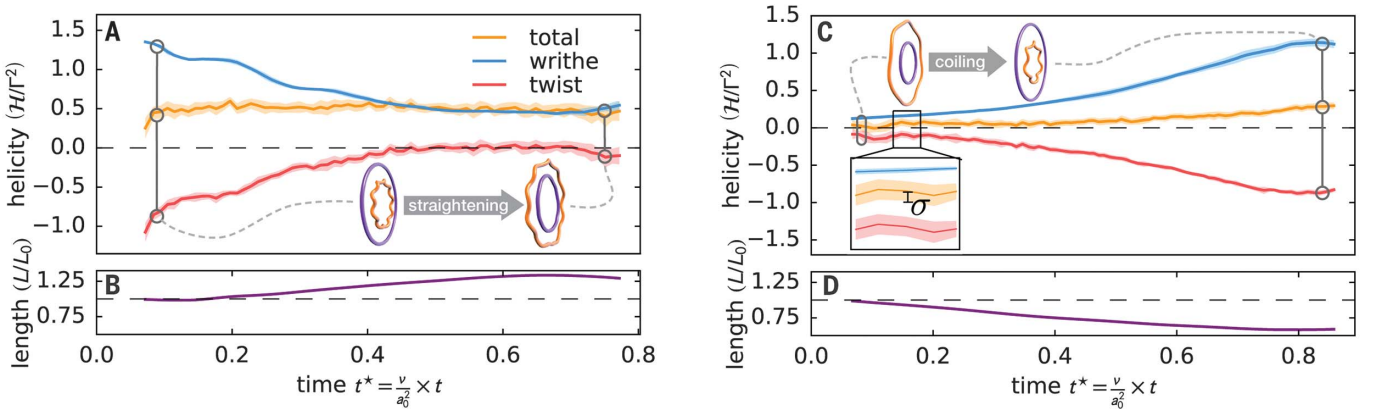

Fig. 3. Helicity is conserved throughout geometric deformations by efficient conversion of writhe to twist. (**A** and **C**) The helicity inside the experimental volume for helix stretching and compression, respectively, over half of a leapfrogging period. The total helicity of the ring-and-helix configuration is computed by integrating the tangential flow along each loop, normalizing by Γ of each loop, and then summing (gold). The writhe of each loop is computed from the traced centerline (blue). The twist is computed by taking $\mathcal{H}/\Gamma^2 - Wr$ (red). The linking is identically zero and thus is omitted. The writhe, linking, and twist of the planar ring are zero throughout the evolution and have been omitted for clarity but are included in the supplementary materials (*41*). Each solid line shows the mean value across 10 [in (A)] and eight [in (C)] different experimental runs, and the shading indicates a standard deviation (σ) across trails in either direction away from this mean. Time is rescaled by ν/a_0^2, where a_0 is taken to be 1.5 mm in all cases. (**B** and **D**) The length of the helix (L) over time, normalized by its initial length (L_0). The length of the corresponding planar ring for each case can be found in the supplementary materials (*41*). (**E**) A schematic demonstrating the geometric mechanism for helicity transfer between writhe and twist as writhe is increased through coiling or decreased through straightening the bundle.

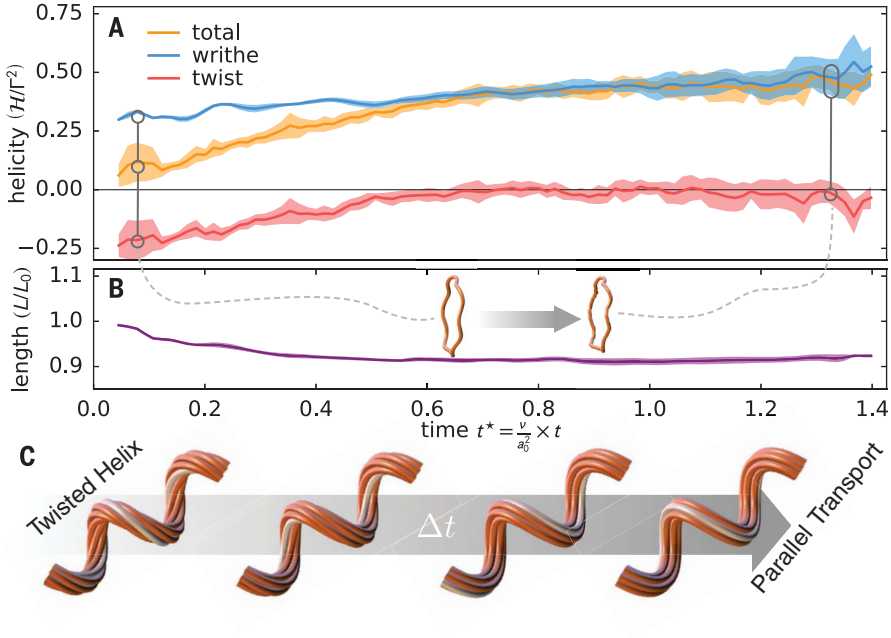

Fig. 4. Helicity tends to writhe. (**A**) The helicity content of an isolated helix, with writhe, twist, and total helicity shown in blue, red, and gold, respectively, computed as described in Fig. 3. The solid lines represent the mean values across 16 total trials, eight of which span the first two-thirds and the remaining eight of which span the second two-thirds of the total duration; shading indicates a standard deviation in either direction. Time is rescaled as in Fig. 3. (**B**) The length of the helix over time, normalized by its initial length. (**C**) A schematic showing the evolution of a twisted bundle over time in the absence of geometric deformation, illustrating the dissipation of twist and attraction to state in which the field lines are parallel-transported along the centerline.

To measure the total helicity from the centerline flow, we created vortices by accelerating three-dimensional (3D)–printed hydrofoils of prescribed geometries in a tank of water (Fig. 2, A and B) (*37*). Once generated, we visualized the vortices by using fluorescent rhodamine dye excited by a 3D high-speed laser-scanning tomography device (*38*). In this approach, the dye is seeded inside the vortex core by first depositing a thin band of dye on the trailing edge of the hydrofoil. On submersion into the fluid, the dye slowly diffuses, positioning it in the region of maximum vorticity generation. By modulating the intensity of the dye pattern on the hydrofoil, small bright dye blobs can be seeded at regular intervals along the less bright centerline path of the vortex (Fig. 2C). This precise illumination patterning results in a collection of passive tracers inside the vortex core (Fig. 2D), the motion

of which can be tracked over time to sample the flow velocity on the centerline (Fig. 2, E to G; Movie 1; and movies S2 and S3). To complete the measurement of the total helicity, we then require only the circulation of the vortices, which we obtain from particle image velocimetry measurements performed on neutrally buoyant tracer particles illuminated by a stationary laser sheet (*39*, *40*). For all experiments, the Reynolds number, defined as Γ/ν (where ν is kinematic viscosity), falls in the range of 12,000 to 20,000.

To probe the possible interaction between writhe and twist, we considered a simple system in which a helically wound vortex loop leapfrogs with a second, planar vortex ring (Fig. 2, F and G). As the pair evolves, the helical loop is periodically stretched (compressed), causing the coils to become looser (tighter) and the writhe to decrease (increase), whereas the planar ring remains writhe-free throughout the evolution (*41*), allowing the investigation of general writhe-changing deformations.

We tracked dye-blob trajectories over half of a leapfrogging period of a helical vortex initially generated within a larger concentric planar vortex ring (Fig. 2F). Tracking the evolving vortex shapes, we measured a sharp decrease in the magnitude of the writhe as the helical vortex is stretched by the flow of the outer vortex ring (Fig. 3A; linking is zero in this case). The total helicity, however, remains roughly constant as its two components vary, indicating compensation of the dramatic change in writhe by the production of twist.

This compensation of changes in writhe by twist production is not limited to instances of decreasing writhe. We compressed a helically wound vortex loop by simultaneously generating a smaller concentric planar ring within it (Fig. 2G). We measured a rapid increase in the writhe along with simultaneous production of negative twist to roughly conserve total helicity (Fig. 3C). Thus, for both increasing and decreasing writhe, changes in writhe are efficiently coupled to equal and opposite twist production.

A simple geometric mechanism characteristic of inviscid flows (*19*, *42*) allows us to understand our observations of the interaction between writhe and twist. During the stretching process, the vortices behave like a coiled telephone cord: Pulling the cord straight to remove the coils results in an equivalent local twist as the parallel transport framing becomes unwound (Fig. 3E). This process had previously been associated with ideal fluids (*19*); our measurements show that it also occurs in viscous flows.

Having demonstrated an inviscid mechanism for the conservation of helicity—the efficient compensation of changes in writhe by corresponding twist production—we turn our attention to helicity dynamics in the absence of external flows. To probe this, we generated an isolated helical loop of comparable size to those used in the previous experiments and followed its evolution over a distance almost twice as long as that used previously, again independently measuring both the writhe and total helicity. We observed that the total helicity is initially nearly zero, indicating that equal and opposite amounts of twist and writhe are present. In the absence of external flows that would deform the helical vortex, the helicity trends away from zero toward the writhe of the helix (Fig. 4A), instead of remaining constant. This convergence of the helicity to the writhe indicates that the twist component of the helicity is dissipated by viscous effects over time, and because, in this case, the twist is negative, the total helicity increases as a result of dissipation. Once viscosity has produced a zero-twist state, the helicity remains roughly constant and equal to the writhe as the helix continues to evolve, indicating that the writhe helicity is protected from viscosity and provides a stable storage mode in the absence of external flows.

We rationalize this process by recalling the geometric origin of the three contributions to helicity: Linking and writhe are nonlocal quantities that require knowledge of the entire path to be computed; twist, in contrast, can be measured locally and thus is the only one that is dissipated by viscosity. We show theoretically that, in the absence of twist, the rate of change of helicity for a writhing vortex is zero (*43*). As a local quantity, the rate of this dissipation process depends on details of the vortex core—the profile shape, degree of uniformity along its length, and twist configuration can all influence how quickly it proceeds—and while those details remain experimentally inaccessible, using numeric simulations to understand the fundamentals of this dissipation represents an exciting avenue for future study.

In the context of this preferential twist dissipation, the writhe takes on a special role among the three modes of helicity storage. Previous experiments have shown that helicity stored as linking is quickly and efficiently converted to writhe through reconnection events (*15*, *44*), whereas we have shown here that in the absence of external flows, the twist will decay. Both of these dynamics privilege writhe as the preferred form of helicity storage, positioning it as an organizing principle for the total helicity. A consequence of this is that even when viscous dynamics dominate, helicity can remain constant.

We have found that viscous vortices use geometric mechanisms characteristic of inviscid flows, such as writhe-to-twist conversion, resulting in helicity conservation, and that even when viscosity is the dominant effect, helicity stored as writhe can be conserved, serving as an attractor for its final value. Ideas of topology and geometry thus capture essential features of vortex dynamics in both inviscid and viscous regimes, through writhe-to-twist conversion and helicity conservation in stable writhe. These ideas may extend to complex flows; for example, in turbulence, where stretching and scale coupling are defining features, helicity could be actively driven from writhe to twist. Taken together, our experiments and findings pave the way for the exploration of the topology of general flows.

REFERENCES AND NOTES

1. H. K. Moffatt, *J. Fluid Mech.* **35**, 117–129 (1969).
2. J. B. Taylor, *Phys. Rev. Lett.* **33**, 1139–1141 (1974).
3. Y. Song, R. L. Lysak, *J. Geophys. Res. Space Physics* **94**, 5273–5281 (1989).
4. M. A. Berger, *Geophys. Astrophys. Fluid Dyn.* **30**, 79–104 (1984).
5. B. B. Kadomtsev, *Sov. J. Plasma Phys.* **1**, 710 (1975).
6. F. L. Waelbroeck, *Phys. Fluids B Plasma Phys.* **1**, 2372–2380 (1989).
7. H. K. Moffatt, A. Tsinober, *Annu. Rev. Fluid Mech.* **24**, 281–312 (1992).
8. H. Aref, I. Zawadzki, *Nature* **354**, 50–53 (1991).
9. H. K. Moffatt, *Proc. Natl. Acad. Sci. U.S.A.* **111**, 3663–3670 (2014).
10. C. E. Liang, R. L. Ricca, D. W. L. Sumners, *Sci. Rep.* **5**, 9224 (2015).
11. S. Kida, M. Takaoka, *Fluid Dyn. Res.* **3**, 257–261 (1988).
12. Y. Kimura, H. K. Moffatt, *J. Fluid Mech.* **751**, 329–345 (2014).
13. M. V. Melander, F. Hussain, in *Center for Turbulence Research, Proceedings of the Summer Program 1988* (Center for Turbulence Research, 1988), pp. 257–286.
14. F. Maggioni, S. Alamri, C. F. Barenghi, R. L. Ricca, *Phys. Rev. E Stat. Nonlin. Soft Matter Phys.* **82**, 026309 (2010).
15. M. W. Scheeler, D. Kleckner, D. Proment, G. L. Kindlmann, W. T. M. Irvine, *Proc. Natl. Acad. Sci. U.S.A.* **111**, 15350–15355 (2014).
16. R. L. Thompson, C. M. Mead, R. Edwards, *Weather Forecast.* **22**, 102–115 (2007).
17. D. K. Lilly, *J. Atmos. Sci.* **43**, 126–140 (1986).
18. E. Levich, E. Tzvetkov, *Phys. Lett. A* **100**, 53–56 (1984).
19. H. K. Moffatt, R. L. Ricca, *Proc. R. Soc. Lond. A* **439**, 411–429 (1992).
20. R. H. Kraichnan, *J. Fluid Mech.* **59**, 745–752 (1973).
21. J. C. André, M. Lesieur, *J. Fluid Mech.* **81**, 187–207 (1977).
22. P. R. Spalart, *Annu. Rev. Fluid Mech.* **30**, 107–138 (1998).
23. T. Gerz, F. Holzäpfel, D. Darracq, *Prog. Aerosp. Sci.* **38**, 181–208 (2002).
24. C. P. Ellington, C. van den Berg, A. P. Willmott, A. L. R. Thomas, *Nature* **384**, 626–630 (1996).
25. M. H. Dickinson, F.-O. Lehmann, S. P. Sane, *Science* **284**, 1954–1960 (1999).
26. S. P. Sane, *J. Exp. Biol.* **206**, 4191–4208 (2003).
27. H. K. Moffatt, S. Kida, K. Ohkitani, *J. Fluid Mech.* **259**, 241–264 (1994).
28. S. Douady, Y. Couder, M. E. Brachet, *Phys. Rev. Lett.* **67**, 983–986 (1991).
29. U. Frisch, A. N. Kolmogorov, *Turbulence: The Legacy of A. N. Kolmogorov* (Cambridge Univ. Press, 1995).
30. M. V. Berry, *Proc. R. Soc. Lond. A* **392**, 45–57 (1984).
31. R. Y. Chiao, Y.-S. Wu, *Phys. Rev. Lett.* **57**, 933–936 (1986).
32. S. Pancharatnam, *Proc. Indian Acad. Sci. A* **44**, 247–262 (1956).
33. A. Tomita, R. Y. Chiao, *Phys. Rev. Lett.* **57**, 937–940 (1986).
34. M. A. Berger, G. B. Field, *J. Fluid Mech.* **147**, 133–148 (1984).
35. Details are given in the supplementary text (Calculation of total helicity).
36. Details are given in the materials and methods (Tracer identification, tracking, and analysis protocol).
37. Details are given in the materials and methods (Hydrofoil shapes and specifications).
38. D. Kleckner, W. T. M. Irvine, *Nat. Phys.* **9**, 253–258 (2013).
39. W. Thielicke, E. Stamhuis, *J. Open Res. Softw.* **2**, e30 (2014).
40. Details are given in the materials and methods (Measuring circulation via PIV).
41. Details are given in the supplementary text (Helicity values of planar loops).
42. H. Pfister, W. Gekelman, *Am. J. Phys.* **59**, 497–502 (1991).
43. Details are given in the supplementary text (Estimating dissipation with dimensional analysis).
44. D. Kleckner, L. H. Kauffman, W. T. M. Irvine, *Nat. Phys.* **12**, 650–655 (2016).

ACKNOWLEDGMENTS

This work was funded by U.S. NSF grant DMR-1351506 and the Packard Foundation. Additional support was provided by the Chicago MRSEC (U.S. NSF grant DMR 1420709), which is also gratefully acknowledged for access to its shared experimental facilities. W.M.v.R. thanks the Swiss National Science Foundation (SNF) for financial support.

SUPPLEMENTARY MATERIALS

www.sciencemag.org/content/357/6350/487/suppl/DC1
Materials and Methods
Supplementary Text
Figs. S1 to S13
References (*45*–*60*)
Movies S1 to S7

30 December 2016; resubmitted 24 April 2017
Accepted 22 June 2017
10.1126/science.aam6897

Complete measurement of helicity and its dynamics in vortex tubes

Martin W. Scheeler, Wim M. van Rees, Hridesh Kedia, Dustin Kleckner and William T. M. Irvine

Science **357** (6350), 487-491.
DOI: 10.1126/science.aam6897

Linking fluids as they twist and writhe

Helicity is a measure of cork-screw-like motion described by the amount of twisting, writhing, and linking in a fluid. Total helicity is conserved for ideal fluids, but how helicity changes in real fluids with even tiny amounts of viscosity has been an open question. Scheeler *et al.* provide a complete measurement of total helicity in a real fluid by using a set of hydrofoils to track linking, twisting, and writhing (see the Perspective by Moffatt). They show that twisting dissipates total helicity, whereas writhing and linking conserve it. This provides a fundamental insight into tornadogenesis, atmospheric flows, and the formation of turbulence.

Science, this issue p. 487; see also p. 448